Analyst

This is an *Accepted Manuscript*, which has been through the Royal Society of Chemistry peer review process and has been accepted for publication.

Accepted Manuscripts are published online shortly after acceptance, before technical editing, formatting and proof reading. Using this free service, authors can make their results available to the community, in citable form, before we publish the edited article. We will replace this *Accepted Manuscript* with the edited and formatted *Advance Article* as soon as it is available.

You can find more information about *Accepted Manuscripts* in the **Information for Authors**.

Please note that technical editing may introduce minor changes to the text and/or graphics, which may alter content. The journal's standard **Terms & Conditions** and the **Ethical guidelines** still apply. In no event shall the Royal Society of Chemistry be held responsible for any errors or omissions in this *Accepted Manuscript* or any consequences arising from the use of any information it contains.

1
2
3
4
5
6
7
8
9
10
11
12
13
14
15
16
17
18
19
20
21
22
23
24
25
26
27
28
29
30
31
32
33
34
35
36
37
38
39
40
41
42
43
44
45
46
47
48
49
50
51
52
53
54
55
56
57
58
59
60

Direct Detection of MicroRNA based on Plasmon Hybridization of Nanoparticle Dimers

Yang Wang[a], Elspeth MacLachlan[b], Bach Kim Nguyen[a], Guodong Fu[b], Chun Peng[b] and Jennifer I. L. Chen[a]*

[a]Department of Chemistry, York University, 4700 Keele Street, Toronto, ON, Canada M3J 1P3

[b]Department of Biology, York University, 4700 Keele Street, Toronto, ON, Canada M3J 1P3

*E-mail: jilchen@yorku.ca

KEYWORDS. Sensing, plasmon hybridization, microRNA, DNA, spectroscopy, biomarkers, nanostructures, complex media

ABSTRACT. MicroRNAs (miRNA) are important for regulating a range of biochemical pathways. Abnormal levels of miRNA in cells or secreted into biological fluids have been identified in diseases. MiRNA can therefore be potential biomarkers for early disease diagnosis; however their detection and quantification are challenging. Herein we apply the sensing platform of discrete actuatable dimers for the detection of human miR-210 (hsa-miR-210-3p). The detection signal is a spectral blue shift in the hybridized plasmon mode as monitored by single-nanostructure spectroscopy. We investigate the specificity and detection limit of the platform and quantify miR-210 levels in RNA extracts of cells cultured under different oxygen tensions. In

addition we demonstrate the feasibility of detection in complex media by examining miR-210 secreted in cell media. This sensing platform may be developed as a bioanalytical tool for validating miRNA profiles of biological fluids.

INTRODUCTION

MicroRNAs (miRNA) are short (ca. 20 nucleotides), non-coding RNAs recently discovered to be important for regulating protein translation and a range of biochemical pathways.[1,2] Abnormal levels of intracellular and extracellular miRNAs (e.g. secreted in blood or urine) have been identified in several diseases including preeclampsia[3,4] and cancer[5-7]. MiRNA are therefore potential biomarkers and therapeutic targets. While thousands of miRNA have been identified, disentangling the role of individual miRNA is challenging because each miRNA can target many messenger RNAs at a time and one messenger RNA can be targeted by many miRNAs. There are only a limited number of analytical methods for the detection and quantification of miRNA[8-12]. The benchmark techniques, including microarrays[13,14] and RT-qPCR[15,16], require miRNA to be purified and transcribed to DNA which is then amplified by polymerase reactions. False positives from contamination are problematic and absolute quantification in general is challenging. As a result, there is a need to develop analytical platforms for the detection and validation of miRNA in complex biological samples.

Discrete plasmonic nanoparticle assemblies have recently emerged as invaluable probes for sensing and imaging applications.[17-20] They provide a wealth of information because of the unique interparticle plasmon coupling effects which can infer biomolecular interactions in cellular environment, as well as providing a means for miniaturized sensing devices that can be easily integrated with microfluidics[17] or other rapid diagnostic methods.[21] Recently we demonstrated a chip-based sensing platform based on dynamically-linked gold nanoparticle

dimers.[22,23] Detection is achieved by monitoring the spectral shift of the localized surface plasmon resonance (LSPR) of dimers anchored on a substrate. Previous proof-of-concept of this sensing scheme examined targets including a synthetic DNA that contains a hairpin structure and a model protein. Herein we show that dimers can be tailored to detect any sequence by modifying the stem-loop linker sequence. We employ single-nanostructure spectroscopy[24,25] to probe the optical response of discrete nanoparticle dimers and investigate the detection limit, selectivity and specificity of this sensing platform. The dimers are applied to the detection of miR-210, which is a biomarker for hypoxia-related diseases and is up-regulated in cells that are deprived of oxygen.[8,26] The detection and quantification of miR-210 levels may allow early diagnosis of hypoxia-related diseases such as preeclampsia – a condition that results in serious complications in 5-8% of pregnant women.[27,28] We quantify the concentrations of miR-210 in RNA extracts from cells cultured under different O_2 levels, and the results are corroborated with conventional RT-qPCR. In addition we demonstrate the feasibility of detecting secreted miR-210 in cell media. The chip-based dimer sensor may present new opportunities for miniaturized sensor and high-density multiplexed detection.

RESULTS AND DISCUSSION

Principle of detection

Scheme 1a depicts our approach. The nanoparticle dimer is linked by stem-loop DNA and anchored on a glass substrate. The loop sequence (22 bases) is chosen to be complementary to miR-210 (see Scheme S1). Upon binding of the target (DNA or RNA), the nanoparticle dimer geometrically extends. The optical signal comes from changes in the energy of the hybridized plasmon mode[29] that result in a spectral shift in the scattered light. In a closely-spaced dimer, the LSPR of individual particle hybridize to form bonding and antibonding plasmon modes (Scheme

1b). The energy of the longitudinal bonding plasmon mode is extremely sensitive to the interparticle separation distance and has therefore been explored as plasmon ruler.[30-33] When the dimer geometrically extends, plasmon coupling is weakened and the scattering peak blue shifts. This spectral blue shift – which is opposite in sign and large in magnitude compared to shifts arising from refractive index changes – has the potential to differentiate target-binding from non-specific adsorption in complex media as demonstrated in our previous work.[22,23]

Optimization of hybridization conditions

The nanoparticle dimers (with particle diameters of 100 nm and 60 nm) scatter light strongly as can be seen in the darkfield microscopy image (Fig. 1a inset). A sample area of ~20 mm^2 is typically prepared, from which dimers within an area of 100x100 μm^2 are examined spectroscopically. Dimers can be distinguished from single nanoparticles or other multi-nanoparticle assemblies by analyzing the polarized scattered light (see Fig. S1); on average dimers account for ~10% of the nanostructures on the substrate (see Table S1). To ensure that the stem-loop sensing motif unzips and fully extends upon target binding, we first examined a DNA sequence that complements both the loop and stem (for a total of 27 bases). The unzipping of the stem-loop structure is found to be very sensitive to the ionic strength of the buffer. Figure 1a shows representative scattering spectra of a nanoparticle dimer before and after exposure to DNA target at optimal hybridization condition (PBS, 0.05 M NaCl) as monitored by single-nanostructure spectroscopy. The peak at 618 nm is attributed to the hybridized bonding plasmon mode, and it shifts by –17 nm to 601 nm when DNA target binds. Figures 1b and c show the distribution of the fractional shifts, defined as the wavelength change divided by the initial LSPR peak position ($\Delta\lambda/\lambda$), of dimers exposed to DNA target at different buffer conditions. For each experiment, the scattering spectra of many dimers on multiple samples were measured (ca. 30

dimers for each sample). A statistical analysis is necessary because the LSPR is sensitive to variations in sizes and shapes of the nanoparticles; additionally the number of DNA linkers for a dimer may also vary. The histogram in figure 1b shows that at high salt concentration (0.3M NaCl), the hybridization of the DNA target with the linker is not effective, possibly due to the high stabilization of the intrastrand stem duplex.[34] By decreasing the salt concentration to 0.05 M NaCl, dimers extend in the presence of DNA target, resulting in a significant spectral blue shift (Fig. 1c). Likewise we optimized the hybridization buffer condition for miR-210 binding; we find that RNA binds more effectively in citrate buffer compared to phosphate buffer[35] (Fig. 1d and e). The fractional shift for a population of 65 dimers upon exposure to synthetic miR-210 in citrate buffer (SSC, 50 mM Na^+) is -0.0180±0.0013, about 11 nm of blue shift in LSPR peak. In comparison, the average fractional shift for dimers exposed to DNA target (PBS, 50 mM Na^+) is -0.0247±0.0018, as summarized in Fig. 1f. The DNA target yields a greater extension than miR-210 because the hybridized duplex is longer (27 vs 22 bases), and that a RNA-DNA duplex is shorter than a DNA-DNA duplex[36] (2.8 Å vs 3.4 Å per base pair). Additionally, the control experiment shows a negligible shift when dimers were exposed to other miRNA (miR-376c, Fig. 1f), conferring the good selectivity.

SPR-based platform had been explored for miRNA detection previously.[37] However, detection required the addition of a duplex-binding antibody to increase the signal because the conventional technique relies on refractive index changes and that very small change of refractive index is induced by RNA binding. In comparison, the hybridized plasmon modes of dimers yield large spectral shifts and enables direct optical detection.

Specificity

One of the main challenges with miRNA detection is specificity. A family of miRNAs (e.g. miRNA-376a, 376b and 376c) has similar sequences with each differing by only a few bases.[38] To determine the specificity of this sensing platform, we introduced one, two or three mismatches to the DNA target sequence (mm1, mm2 and mm3, respectively). The mismatch position is placed at the center of the loop sequence (see Scheme S1). Figure 2a summarizes the average fractional shifts for dimers exposed to perfect DNA complement (cDNA) vs the mismatched sequences at micromolar concentrations. The cDNA yields a shift of -0.0247±0.0018, while mm1, mm2 and mm3 exhibit shifts of -0.0129±0.0010, -0.0083±0.0010 and -0.0011±0.0010 (histograms shown in Fig. 2b - d). A decrease in the magnitude of the shift is observed as the number of mismatched bases increases. This observation is in line with the expected decrease in the stability of the duplex with increasing non-complementarity of the hybrid.[39] Notably, dimers exposed to mm3 show a negligible average shift, essentially discriminating this sequence completely under the buffer condition we used. The results demonstrate that dimers can effectively differentiate between similar sequences when the amount of targets is in excess. Further optimization of the hybridization condition may enhance the discrimination between single base mismatch and perfect complement.

Detection range for miR-210

Next we investigate the detection range of the dimer sensing platform for the quantification of cellular miR-210. The calibration curve in Figure 3a shows an exponential-relation of average fractional shift to the concentration of synthetic miR-210 (the linear logarithmic plot is shown in the inset). The exponential-like relation may arise from the d^{-3} distance-dependence of plasmon coupling[30] (where d is the interparticle separation). Under optimal buffer condition, we can detect miR-210 down to tens of femtomolar, which corresponds to attomole (10^{-18}) of miRNA

for a sample volume of 60 μL. The sub-picomolar detection range is plausible because of the high binding affinity of oligonucleotides on AuNP ($\sim 10^{18}$ for 21-mer[40]) and the low concentration of stem-loop probe strands from dimers anchored on the substrate. We estimate the sample to contain 10^7 probe strands, within an order of the amount of analyte present. In addition, the spectral shift originates from binding of the target to the linkers in the nanoparticle junction area only, and hence a fraction of the total binding can induce a detection signal. We conservatively estimate the detection limit to be 0.009 pM by considering that the standard error of the mean on the average fractional shift is typically 0.0015 and that detection limit signal is 3σ. The uncertainty can be decreased further by examining a larger set of dimers; hence the detection limit may be improved by using a high-throughput spectral acquisition instrument such as a hyperspectral imaging microscope.[41] The calibration curve shows that the working range is limited as it spans only an order of concentrations with the signal saturating at 0.1 pM. Quantitative detection may therefore require serial additions of the analyte to avoid saturation of the signal.

Quantification of cellular miR-210 levels

We now quantify the levels of cellular miR-210 to validate the dimer sensing platform. We cultured trophoblast cells under different oxygen tensions (21% vs 3% O_2) and extracted the total RNA. The level of miR-210 is up-regulated under hypoxic condition, where cells are exposed to 3% instead of 21% O_2.[42] Figure 4a and b show the histogram of the fractional shifts for dimers exposed to RNA extracts from cells grown under normoxic (21% O_2) and hypoxic (3% O_2) conditions. The hypoxic sample exhibits a fractional shift of -0.0144±0.0011 compared to -0.0117±0.0011 for normoxic sample. We carried out the experiment for additional batches of RNA extracts as summarized in Table 1. A comparison of the average levels of miR-210 under

different oxygen tensions obtained from dimer sensors vs RT-qPCR is shown in Fig. 4c. We obtain 59±13 copies of miR-210 per cell for normoxic cells compared to 134±9 copies for hypoxic cells from the dimer sensing platform. Note that these values assume 100% extraction and purification efficiency and hence are lower limits. The dimers show an increase of 2.27±0.0.93-fold (N = 7) of miR-210 levels for hypoxic vs normoxic cells, compared to a ratio of 3.54±1.98 (N = 6) from PCR. The results are statistically the same (t(11) = 1.52, p > 0.05). The agreement demonstrates the feasibility of the dimer sensing platform for the quantification of cellular miR-210. When combined with surface patterning, discrete nanostructure-based sensors may provide the basis for ultra-high density multiplexed arrays for biomarker profiling as the sensing area for one target is ~10000 μm^2.

Direct detection of miR-210 in complex media

Lastly we explore the detection of miR-210 in cell medium using the nanoparticle dimers. Cells excrete miRNAs and other biomolecules during growth,[43] so we collected the cell media after incubation for 2 days to investigate the potential of dimers to detect miR-210 in complex media. We compare the spectral shift of dimers linked by different probe DNAs upon exposure to as-cultured cell medium and also cell medium spiked with excess miR-210 (Fig. 5). Dimers that target miR-210 show a significant blue shift of -0.0082±0.0009 when exposed to cell medium spiked with excess miR-210, conferring the ability to detect miR-210 based on the blue-shift spectroscopic signature. The magnitude of the shift is smaller in cell medium than in buffer because of the increase in refractive index by the non-specifically adsorbed interfering species. When exposed to as-cultured cell medium, the miR-210 targeting dimers show a fractional shift of -0.0065±0.0012 suggesting the presence of secreted cellular miR-210, which was confirmed by RT-qPCR. In contrast, dimers linked by a non-targeting hairpin structure show a red shift

(0.0114±0.0009), as do non-targeting single nanoparticles (0.0126±0.0009). Figure 5b shows the different distribution of the fractional shifts for miR-210 targeting dimer vs control dimer upon exposure to cell medium. The red shifts in the control experiments suggest non-specific adsorption of proteins or other species in the cell media onto the nanoparticle surface. Although the magnitude of the shift arising from the geometric extension of the dimer is smaller in cell medium than in buffer, absolute quantification can be achieved by establishing a calibration curve in the complex medium of interest.

The spectral blue shift of the miR-210 dimers demonstrates the ability to spectroscopically differentiate miR-210 in the presence of interfering species. However, very high level of interferences (e.g. 75% serum[22] or cell lysates) can yield a substantial red shift from refractive index changes that can mask the spectral blue shift from the extension of the dimer. As a result, crude purification may be required for analyzing complex samples with high protein content while the detection in biological fluids such as plasma and urine, in which circulatory miRNAs have been found, may be achieved directly.

EXPERIMENTAL

Materials

100 nm and 60 nm diameter colloidal gold nanoparticle (AuNP) solutions were purchased from BB international. Anhydrous ethanol and 2-propanol were obtained from Commercial Alcohol. All chemicals were purchased from Sigma Aldrich. Micro Biospin Chromatography Columns and SecureSeal hybridization chamber (13 mm in diameter, 0.8 mm in depth) were purchased from BioRad and Grace Bio-lab, respectively. All water used was deionized to 18 MΩ with Millipore filtration system.

The DNA and RNA sequences were synthesized and HPLC-purified by Integrated DNA Technologies. Thiolated oligonucleotides were treated with disulfide cleavage buffer (0.17M phosphate, 0.1M dithiothreitol, pH 8) and desalted using Micro Biospin Chromatography Columns prior to use.

Oligonucleotide sequences

MiR-210 targeting *dimer (see Scheme S1)*

Seq 1. 5'-HS-AAA AAA AAA AAT GCG ATG CGT T-3' (for 100 nm AuNP)

Seq 2. 5'-HS-AAA AAA AAA ACC GTC TCA GCC GCT GTC ACA CGC ACA GGA CGG AAC GCA TCG CAT-3' (for 60 nm AuNP)

Seq 3 (miR-210). 5'-CUG UGC GUG UGA CAG CGG CUG A-3'

Seq 4 (cDNA). 5'-CCG TCC TGT GCG TGT GAC AGC GGC TGA-3'

Seq 5 (mm1 DNA). 5'-CCG TCC TGT GCG TGT GAT AGC GGC TGA-3'

Seq 6 (mm2 DNA). 5'-CCG TCC TGT GCG TGT GCT AGC GGC TGA-3'

Seq 7 (mm3 DNA). 5'-CCG TCC TGT GCG TGT TCT AGC GGC TGA-3'

Seq 8 (miRNA-376c). 5'-GGU GGA UAU UCC UUC UAU GUU-3'

Control dimer (hairpin structure, see ref. 22)

Seq 9. 5'-HS-AAA AAA AAA ACG CAT TCA GGA T-3' (for 100 nm AuNP)

Seq 10. 5'-HS-TCT CAA CTC GTA CGC ATG ATT GTT TTC AAT CAT GCG CGA AAG ATC CTG AAT GCG-3' (for 60 nm AuNP)

PCR reference

10

U48. 5'-AGU GAU GAU GAC CCC AGG UAA CUC UGA GUG UGU CGC UGA UGC CAU

CAC CGC AGC GCU CUG ACC-3'

Preparation of DNA-functionalized 100 nm AuNP on glass substrate

Glass cover slips (VWR micro cover galss 25 mm × 25 mm) were plasma cleaned (Harrick's

PDC-32G) and immersed in 60 mL anhydrous ethanol with 0.5% APTMS for 2 hours to achieve

amino functional groups on the surface. A volume of 10 µL of water was placed on the centre of

substrate, followed by 10 µL of 100 nm AuNP. The solution was left for 5 minutes to allow the

AuNP to adhere to the glass cover slips. The sample was then rinsed with water and dried. The

coverage of AuNP on substrate was checked under an optical microscope (Nikon Eclipse,

TE2000-U) and a glass scribe gently marked the area of interest. Then, the sample was plasma

treated for 30 seconds and a clean SecureSeal was placed on the substrate to stamp out the area

of interest. A volume of 10 µL of 0.01M PBS, 1 M NaCl, and 0.1% SDS was added to the

sample, followed by 10 µL of 1 µM DNA sequence 1. The sample was kept in a humid box and

incubated for 1 hour. After 1 hour, the sample was rinsed thoroughly with a solution of 0.01M

PBS and 0.05% SDS, then 0.3 M ammonium acetate, and dried with compressed air.

Preparation of DNA-functionalized 60 nm colloidal AuNP

A volume of 300 µL of filtered 60 nm colloidal AuNP solution was concentrated to 100 µL

and added to 100 μL of DNA sequence 2 in water (0.35 O.D. at 260 nm) that has been annealed

at 60 ^{o}C for 10 minutes. The solution was raised to 0.01 M PBS and 0.01% SDS by using 0.1M

PBS and 1% SDS stock solution, respectively, followed by vortexing and sonication and

subsequently left for 20 minutes. Then, the concentration of NaCl was gradually brought to 0.4

M using 0.1 M PBS, 2 M NaCl, and 0.01% SDS stock solution, in increments of 0.05 M each

time. After each addition, the sample was vortexed and sonicated and left for 20 minutes. The

sample was incubated overnight once the concentration of NaCl reached to 0.4 M. The AuNP was then centrifuged and redispersed in 300 μL of 0.01% SDS twice and finally redispersed in a solution composed of 0.01 M PBS, 0.05 M NaCl, 0.01% SDS, and 0.01% azide. The DNA-functionalized 60 nm AuNP solution was stored at 4 ℃ in the dark. Prior to dimerization, the colloidal DNA-AuNP was annealed for 10 minutes at 60 °C and slowly cooled to ensure the stem-loop formation.

Dimerization of DNA-functionalized 100 nm and 60 nm AuNP

A volume of 10 μL of solution containing 0.01 M PBS, 0.3 M NaCl, 0.1% SDS was placed on the substrate where DNA-functionalized 100 nm AuNP was bound (see previous step). Then, a drop of 10 μL of DNA-functionalized 60 nm AuNP solution was added and left for 5 minutes to allow the hybridization to occur. After hybridization, the sample was rinsed with a solution of 0.01M PBS and 0.05% SDS, then 0.3 M ammonium acetate, and dried with compressed air. Darkfield images were taken before and after hybridization. Dimers were confirmed by their anisotropic scattering using polarized darkfield spectroscopy (Fig. S1).

Sensing experiments

The dimers were incubated in PBS (with specified concentration of NaCl) or 50 mM citrate buffer (0.3X SSC), using a SecureSeal hybridization chamber (13 mm in diameter, 0.8 mm in depth). A total volume of ~55 μL of solution can be pipetted into the chamber through 1.5 mm ports. The dimers were incubated for at least 2 hours (typically overnight) before collecting the darkfield scattering spectra in buffer. For sensing experiments, volumes of 10 - 30 μL of analyte solutions (at the same buffer condition) were added and incubated for at least 2 hours, typically overnight. All solutions were filtered with cellulose acetate syringe filter (0.2 μm) prior to

addition. The peak positions of the scattering spectra were analyzed by peak-fitting (Lorentzian) using Igor Pro software.

Single-Nanostructure Spectroscopy set up

Single-nanostructure optical microscopy and spectroscopy were carried out using a Nikon TE-2000U inverted microscope fitted with a transmitted darkfield condenser and a 60X objective with an intermediate 1.5X lens (total magnification 90X). The output of the microscope was directed either to a thermoelectrically-cooled CCD camera (Jenoptik) or to a fiber optic cable (diameter = 100 μm) connected to a portable charge-coupled device spectrometer (USB2000, Ocean Optics). A standard tungsten halogen lamp was used for transmitted darkfield illumination and a home-made rotating stage with a linear polarizer was used when analyzing the polarization of scattered light.

Data analysis

The position of the plasmon resonances was obtained by fitting the data (with spectral range ~100 nm near the peak of interest) with Lorentzian peak function using Igor program. The errors reported on fractional shifts are standard error of the mean.

Cell Culture

Human trophoblast HTR8/SVneo cells were obtained and cultured as previously reported.[44] Briefly, cells were cultured in RPMI-1640 media supplemented with 10% heat-inactivated fetal bovine serum, 100 U/mL penicillin and 100 mg/mL streptomycin. Cells were seeded in 6 or 12 well plates and incubated overnight at 37 °C in 5% carbon dioxide and 21% oxygen. The cells were then washed briefly with PBS and incubated in fresh media for 48 hours at 37 °C in 5% carbon dioxide with either 21% or 3% oxygen. The cell media from normoxic condition (21%

O$_2$) was collected and centrifuged for five minutes at 16,000 g to remove any cells. A volume of 30 µL of cell medium adjusted to the buffer condition was injected for sensing experiments.

Total Cellular RNA Extraction

Total RNA was extracted from cultured cells using TRIzol reagent (Invitrogen) following manufacturer's protocol with minor modifications.[45] Cell media was removed and 1 mL of TRIzol reagent was added to each well. The solution was pipetted up and down several times to lyse the cells, and then collected and stored overnight at -80 °C. After thawing the samples, 0.2 mL chloroform was added to each tube, vortexed briefly, and incubated at room temperature for 3 minutes. The samples were then centrifuged at 12,000 g for 15 minutes at 4 °C. The aqueous phase was removed and saved. 0.5 mL 100 % isopropanol was added to the aqueous phase, and incubated for 30 minutes at -80 °C. Once thawed, the samples were centrifuged for 10 minutes at 12,000 g at 4°C. The supernatant was removed, and the RNA pellet was washed twice with 75% ethanol, and once with 100 % ethanol. Each wash was followed by centrifugation at 7,500 g for five minutes at 4°C. The pellet was air dried, and dissolved in 17 µL of DEPC treated water. RNA concentration was determined using NanoDrop 2000 (Thermo Scientific). RNA quality was assessed by gel electrophoresis and UV-Vis.

Total Extracellular RNA Extraction

Total RNA was extracted from cultured cell medium using TRIzol LS reagent (Invitrogen) following manufacturer's protocol with minor modifications.[44] 1.2 mL TRIzol LS was added to 400µL cell medium with all cells removed. Total RNA was then extracted following the same protocol used to extract total cellular RNA.

Quantitative Reverse Transcription Polymerase Chain Reaction

Relative miR-210 levels were quantified using RT-qPCR, following TaqMan MicroRNA Assays protocol. A volume of 50 ng of total RNA was reverse transcribed into cDNA using a TaqMan miR-210 specific RT primer (Life Technologies). qPCR was performed using TaqMan Small RNA Assays (Life Technologies) with the Rotor-Gene Q real-time PCR cycler (Qiagen). The efficiency of qPCR in the relevant concentration range was calibrated by obtaining the C_t values of diluted RNA extracts and U48 was used as the reference.

CONCLUSIONS

In summary, we demonstrate the application of actuatable nanoparticle dimer sensors for the detection of micro-RNA. The ultra-low sub-picomolar detection range allows the direct quantification of micro-RNA extracted from cells without any amplification. We envision the submicron footprint of the discrete nano optical sensors may enable high density multiplexed detection of tens of miRNAs for validation of miRNA fingerprint for early diagnosis and profiling of diseases. The spectral analysis of discrete reconfigurable multi-nanoparticle assemblies on array chips may be a promising bioanalytical tool.

ACKNOWLEDGMENTS

Supporting Information. Electronic Supplementary Information (ESI) available. See DOI: 10.1039/b000000x

REFERENCES

1. E. Wienholds, W. P. Kloosterman, E. Miska, E. Alvarez-Saavedra, E. Berezikov, E. de

    Bruijn, H. R. Horvitz, S. Kauppinen and R. H. A. Plasterk, *Science*, 2005, **309**, 310-311.

2. D. P. Bartel, *Cell*, 2004, **116**, 281-297.

3. D. A. Enquobahrie, D. F. Abetew, T. K. Sorensen, D. Willoughby, K. Chidambaram and

    M. A. Williams, *Am. J. Obstet. Gynecol.*, 2011, **204**, 178.e12-21.

4. X. M. Zhu, T. Han, I. L. Sargent, G. W. Yin and Y. Q. Yao, *Am. J. Obstet. Gynecol.*,

    2009, **200**, 661-667.

5. S. Volinia, G. A. Calin, C. G. Liu, S. Ambs, A. Cimmino, F. Petrocca, R. Visone, M.

    Iorio, C. Roldo, M. Ferracin, R. L. Prueitt, N. Yanaihara, G. Lanza, A. Scarpa, A.

    Vecchione, M. Negrini, C. C. Harris and C. M. Croce, *Proc. Natl. Acad. Sci. U. S. A.*,

    2006, **103**, 2257-2261.

6. H. Yang, W. Kong, L. He, J. J. Zhao, J. D. O'Donnell, J. Wang, R. M. Wenham, D.

    Coppola, P. A. Kruk, S. V. Nicosia and J. Q. Cheng, *Cancer Res.*, 2008, **68**, 425-433.

7. Y. Shimono, M. Zabala, R. W. Cho, N. Lobo, P. Dalerba, D. Qian, M. Diehn, H. Liu, S.

    P. Panula, E. Chiao, F. M. Dirbas, G. Somlo, R. A. Pera, K. Lao and M. F. Clarke, *Cell*,

    2009, **138**, 592-603.

8. G. D. Fu, J. Brkic, H. Hayder and C. Peng, *Int. J. Mol. Sci.*, 2013, **14**, 5519-5544.

9. A. Valoczi, C. Hornyik, N. Varga, J. Burgyan, S. Kauppinen and Z. Havelda, *Nucleic

    Acids Res.*, 2004, **32**, e175.

10. A. H. Alhasan, D. Y. Kim, W. L. Daniel, E. Watson, J. J. Meeks, C. S. Thaxton and C. A.

    Mirkin, *Anal. Chem.*, 2012, **84**, 4153-4160.

11. D. W. Wegman and S. N. Krylov, *Trac-Trends in Ana.l Chem.*, 2013, **44**, 121-130.

12.   D. W. Wegman and S. N. Krylov, *Angew. Chem. Int. Ed.*, 2011, **50**, 10335-10339.

13.   L. P. Lim, N. C. Lau, P. Garrett-Engele, A. Grimson, J. M. Schelter, J. Castle, D. P. Bartel, P. S. Linsley and J. M. Johnson, *Nature*, 2005, **433**, 769-773.

14.   J. F. Mouillet, T. Chu, D. M. Nelson, T. Mishima and Y. Sadovsky, *FASEB*, 2010, **24**, 2030-2039.

15.   C. F. Chen, D. A. Ridzon, A. J. Broomer, Z. H. Zhou, D. H. Lee, J. T. Nguyen, M. Barbisin, N. L. Xu, V. R. Mahuvakar, M. R. Andersen, K. Q. Lao, K. J. Livak and K. J. Guegler, *Nucleic Acids Res.*, 2005, **33**, e179.

16.   R. B. Donker, J. F. Mouillet, D. M. Nelson and Y. Sadovsky, *Mol Hum Reprod*, 2007, **13**, 273-279.

17.   J. R. Waldeisen, T. Wang, B. M. Ross and L. P. Lee, *ACS Nano*, 2011, **5**, 5383-5389.

18.   J. Wang, S. V. Boriskina, H. Y. Wang and B. M. Reinhard, *ACS Nano*, 2011, **5**, 6619-6628.

19.   A. Wax and K. Sokolov, *Laser & Photonics Reviews*, 2009, **3**, 146-158.

20.   J. Aaron, K. Travis, N. Harrison and K. Sokolov, *Nano Lett.*, 2009, **9**, 3612-3618.

21.   K. Li, W. Qin, F. Li, X. Zhao, B. Jiang, K. Wang, S. Deng, C. Fan and D. Li, *Angew. Chem. Int. Ed.*, 2013, **52**, 11542-11545.

22.   J. I. L. Chen, Y. Chen and D. S. Ginger, *J. Am. Chem. Soc.*, 2010, **132**, 9600-9601.

23.   J. I. L. Chen, H. Durkee, B. Traxler and D. S. Ginger, *Small*, 2011, **7**, 1993-1997.

24.   L. J. Sherry, R. Jin, C. A. Mirkin, G. C. Schatz and R. P. Van Duyne, *Nano Lett.*, 2006, **6**, 2060-2065.

25.   Y. Chen, K. Munechika and D. S. Ginger, *Nano Lett.*, 2007, **7**, 690-696.

26.   S. Y. Chan and J. Loscalzo, *Cell Cycle*, 2010, **9**, 1072-1083.

27. L. Ghulmiyyah and B. Sibai, *Semin Perinatol*, 2012, **36**, 56-59.

28. S. Muralimanoharan, A. Maloyan, J. Mele, C. Guo, L. G. Myatt and L. Myatt, *Placenta*, 2012, **33**, 816-823.

29. P. Nordlander, C. Oubre, E. Prodan, K. Li and M. I. Stockman, *Nano Lett.*, 2004, **4**, 899-903.

30. P. K. Jain, W. Huang and M. A. El-Sayed, *Nano Lett.*, 2007, **7**, 2080-2088.

31. C. Sonnichsen, B. M. Reinhard, J. Liphardt and A. P. Alivisatos, *Nature Biotech.*, 2005, **23**, 741-745.

32. B. M. Reinhard, M. Siu, H. Agarwal, A. P. Alivisatos and J. Liphardt, *Nano Lett.*, 2005, **5**, 2246-2252.

33. L. L. Yang, H. Y. Wang, B. Yan and B. M. Reinhard, *J. Phys. Chem. C*, 2010, **114**, 4901-4908.

34. R. Owczarzy, Y. You, B. G. Moreira, J. A. Manthey, L. Huang, M. A. Behlke and J. A. Walder, *Biochemistry*, 2004, **43**, 3537-3554.

35. E. T. Bolton and C. B. Mc, *Proc. Natl. Acad. Sci. U. S. A.*, 1962, **48**, 1390-1397.

36. N. C. Horton and B. C. Finzel, *J. Mol. Biol.*, 1996, **264**, 521-533.

37. H. Šípová, S. Zhang, A. e. M. Dudley, D. Galas, K. Wang and J. i. Homola, *Anal. Chem.*, 2010, **82**, 10110-10115.

38. Y. Kawahara, B. Zinshteyn, P. Sethupathy, H. Iizasa, A. G. Hatzigeorgiou and K. Nishikura, *Science*, 2007, **315**, 1137-1140.

39. S. H. Ke and R. M. Wartell, *Nucleic Acids Res.*, 1993, **21**, 5137-5143.

40. A. K. R. Lytton-Jean and C. A. Mirkin, *J. Am. Chem. Soc.*, 2005, **127**, 12754-12755.

41. J. M. Bingham, K. A. Willets, N. C. Shah, D. Q. Andrew and R. P. Van Duyne, *J. Phys. Chem. C*, 2009, **113**, 16839-16842.

42. D. Gou, R. Ramchandran, X. Peng, L. Yao, K. Kang, J. Sarkar, Z. Wang, G. Zhou and J. U. Raj, *Am. J. Physiol. Lung Cell. Mol. Physiol.*, 2012, **303**, L682-691.

43. A. Turchinovich, L. Weiz and B. Burwinkel, *Trends Biochem. Sci.*, 2012, **37**, 460-465.

44. G. Fu, G. Ye, L. Nadeem, L. Ji, T. Manchanda, Y. Wang, Y. Zhao, J. Qiao, Y. L. Wang, S. Lye, B. B. Yang and C. Peng, *Hypertension*, 2013, **61**, 864-872.

45. G. Ye, G. Fu, S. Cui, S. Zhao, S. Bernaudo, Y. Bai, Y. Ding, Y. Zhang, B. B. Yang and C. Peng, *J. Cell Sci.*, 2011, **124**, 359-368.
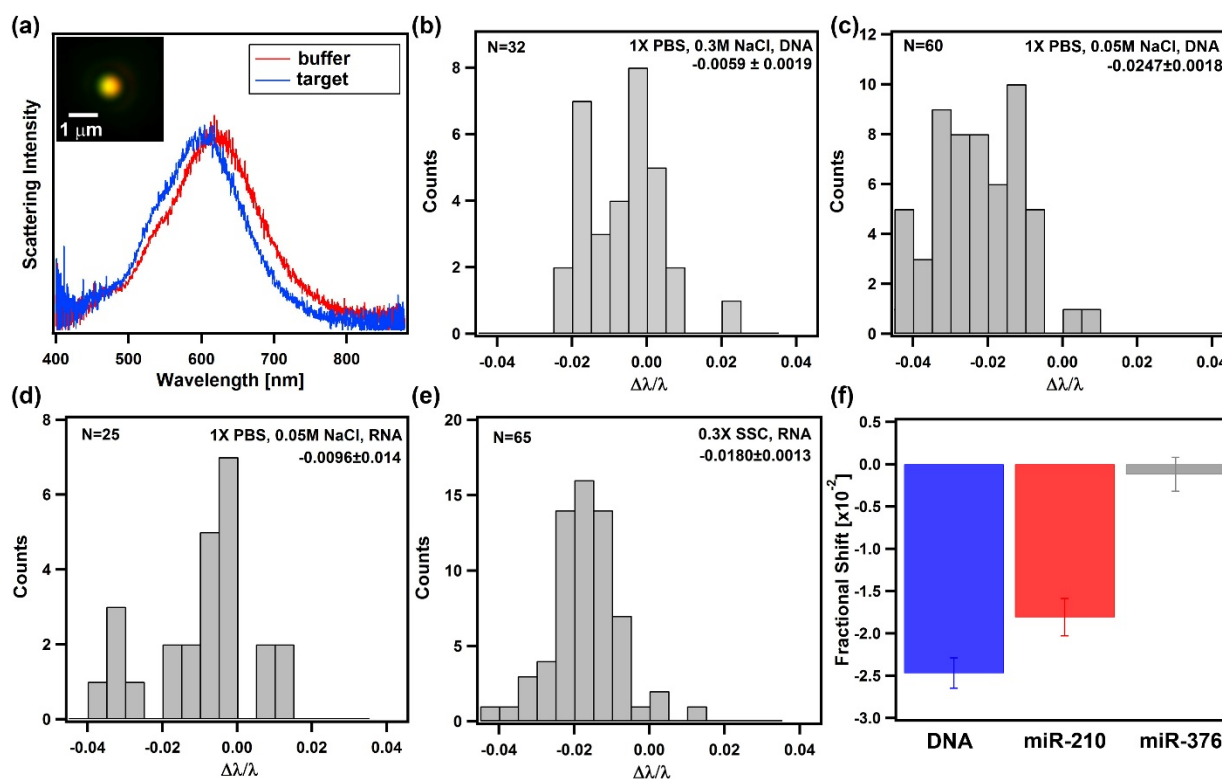
FIGURES

Figure 1. Optical detection of miR-210 and DNA with dimers. (a) Scattering spectra of a dimer before and after exposure to target DNA in PBS and 50 mM NaCl. The inset shows a darkfield image of the dimer. Histograms of fractional shifts for dimers exposed to DNA and RNA targets under different buffer conditions: (b) DNA target (seq. 4) in PBS and 0.3 M NaCl; (c) DNA target in PBS and 50 mM NaCl; (d) miR-210 (seq. 3) in PBS and 50 mM NaCl; and (e) miR-210 in sodium citrate buffer (SSC, 50 mM Na$^+$). The average fractional shifts show that the stem-loop structure opens at low ionic strength (50 mM Na$^+$) but not effectively at high ionic strength (0.3 M Na$^+$). The binding of miR-210 to the DNA linkers on the nanoparticles is further enhanced in sodium citrate buffer ($\Delta\lambda/\lambda$ of -0.0096 ± 0.014 in PBS vs -0.0180± 0.0013 in SSC). (f) A comparison of the fractional shifts of dimers exposed to target DNA, miR-210 and non-target miR-376c-3p under optimal hybridization conditions.
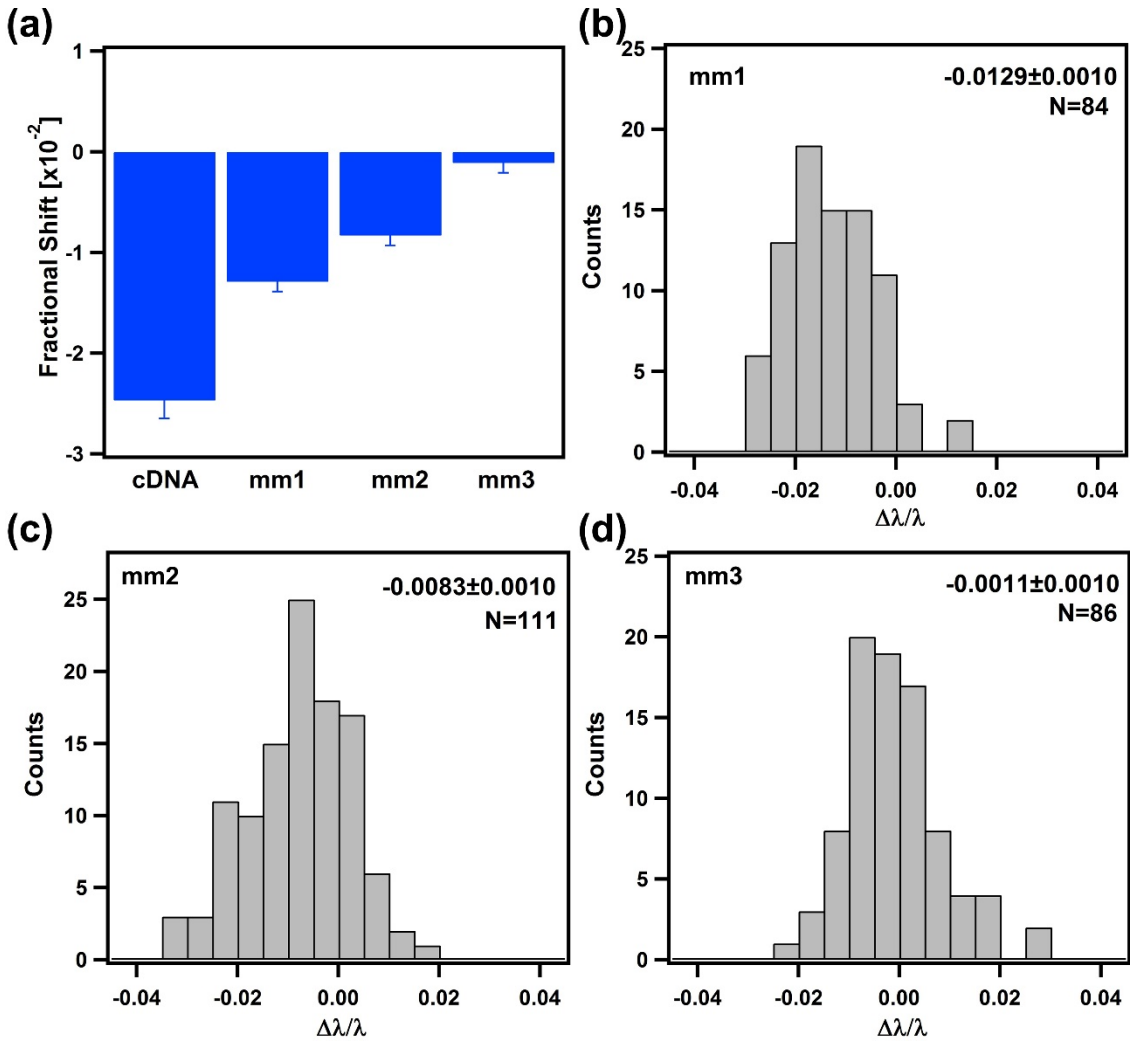
Figure 2. (a) Average fractional shifts of dimers incubated with perfect DNA complement (cDNA) and sequences with different number of mismatches (one, two or three denoted as mm1, mm2 and mm3) in PBS with 50 mM NaCl. Distribution of fractional shifts for dimers exposed to mm1 (b), mm2 (c) and mm3 (d).
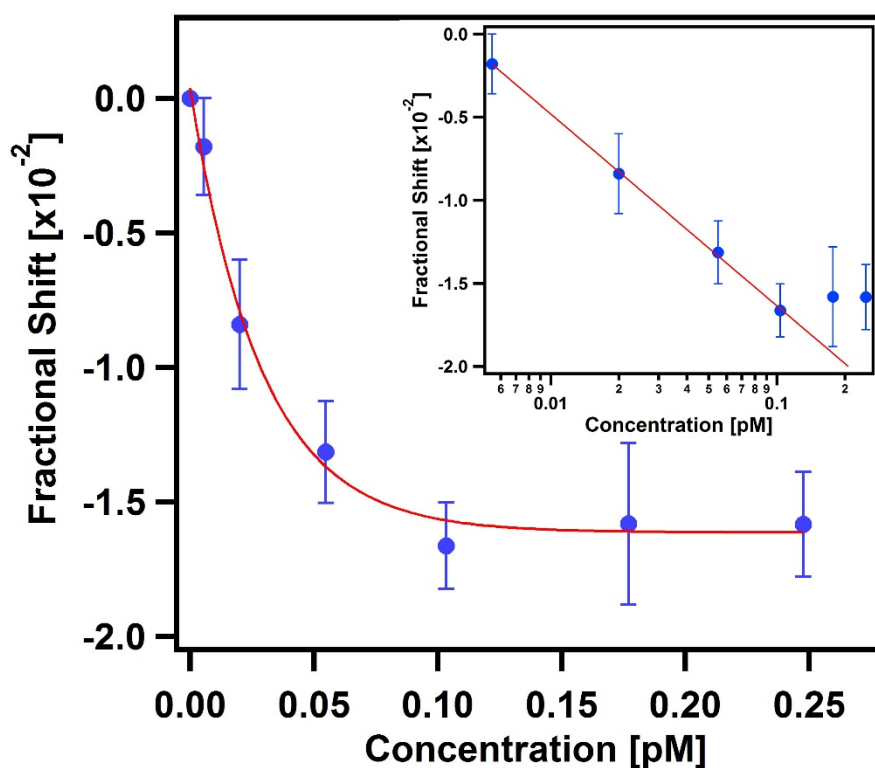
Figure 3. Concentration dependence of the fractional shift on miR-210 in SSC (50 mM Na$^+$). An exponential-relation is observed with a fit of y = 0.0165exp(-34.78x)-0.0161. The inset shows the calibration curve in logarithmic scale (y = -0.0279 – 0.0115 log(x)).
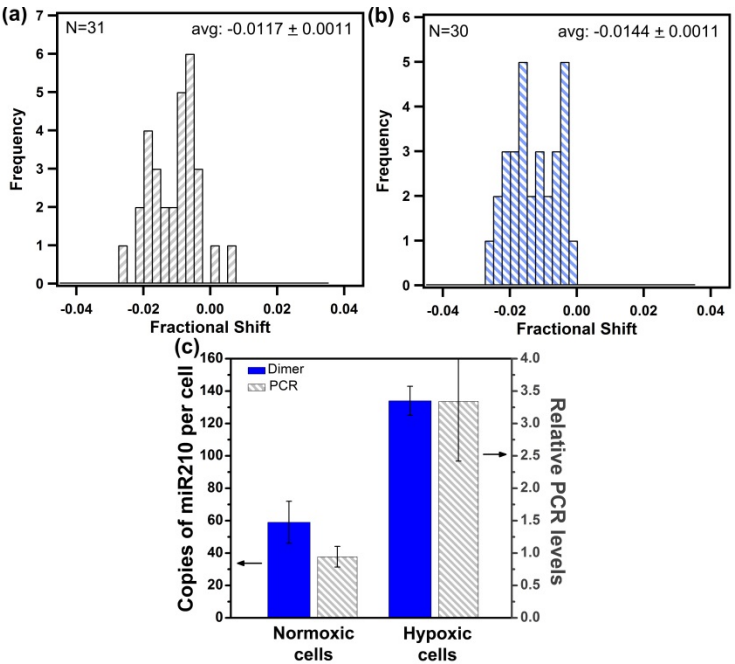
Figure 4. Distribution of fractional shift for dimers exposed to RNA extract of (a) normoxic cells and (b) hypoxic cells in SSC (50mM Na$^+$). The number of copies of miRNA is calculated using the calibration curve. (c) Absolute quantification of miR-210 levels from dimer sensors compared to the relative levels of miR-210 determined by RT-qPCR, normalized to U48 levels. Multiple batches of RNA extracts were analyzed (Table 1) and the error bars represent standard error of the mean.
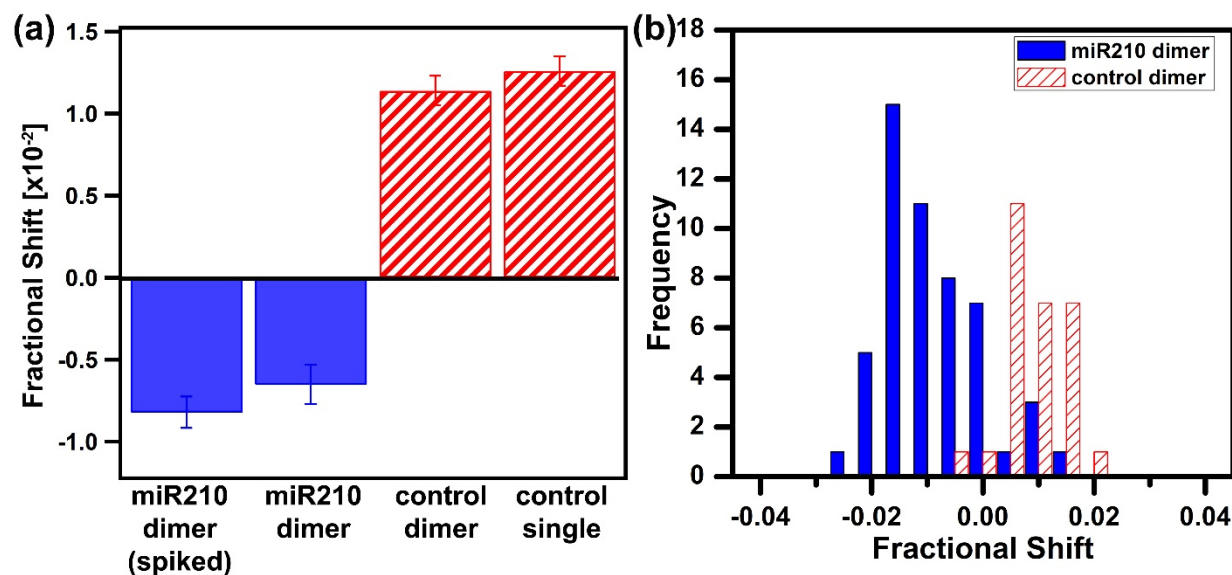
Figure 5. A comparison of fractional shifts of samples exposed to cell media collected after 2 days of cell culturing. (a) Average fractional shifts of miR-210 targeting dimer, control dimer and control single nanoparticle; and (b) histograms of distribution for miR-210 targeting dimer vs control dimer exposed to as-cultured cell media. The results are averaged over three replicates for each cell medium study.
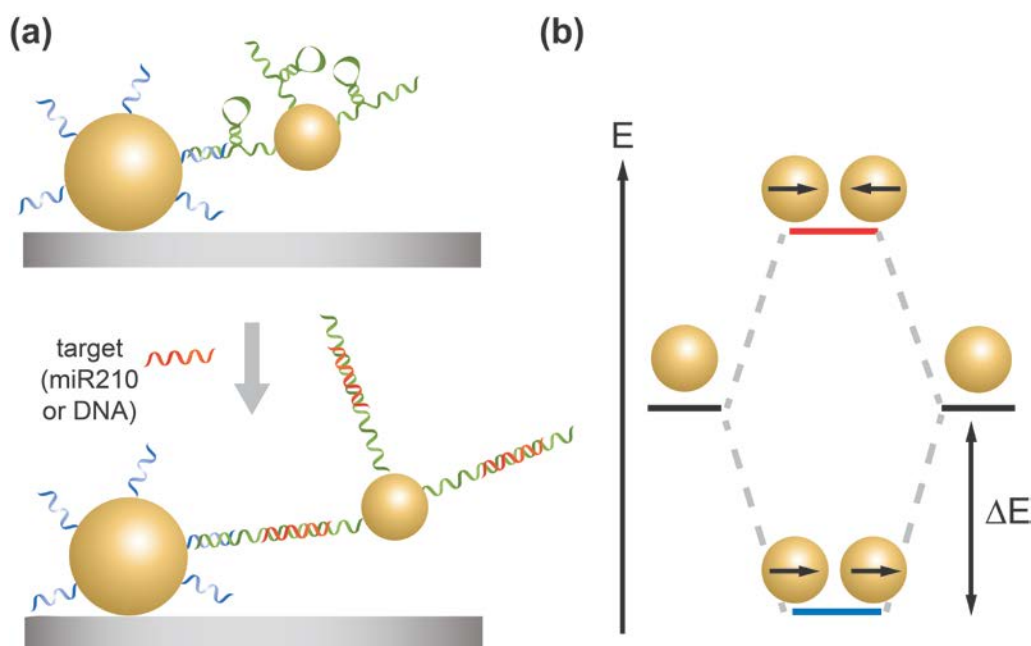
TABLE

Table 1. Data on miR-210 levels in normoxic and hypoxic cells obtained from dimer sensing experiments. The number of miR-210 copies per cell was calculated from the concentration of miR-210 detected by the dimers (in 55 μL), the amount of total RNA added and the amount of total RNA extracted from 50000 cells.

	Total RNA extracted (ng)	Total RNA added (ng)	Fractional shift	Concentration of miR-210 (pM)	# of miR-210 /cell
Normoxic (21% O$_2$)	2878	1000	-0.0117	0.0390	74
	2057	400	-0.0085	0.0206	70
	1334	900	-0.0110	0.0339	33
Hypoxic (3% O$_2$)	3848	877	-0.0123	0.0440	128
	3505	1000	-0.0144	0.0670	156
	1884	400	-0.0113	0.0360	112
	1884	700	-0.0152	0.0786	140

Analyst Accepted Manuscript

25

SCHEMES

Scheme 1. Stem-loop DNA-linked nanoparticle dimer sensing motif and energy diagram of

plasmon hybridization.[a]

[a] Dimer geometrically extends upon binding to target resulting in an increase in the energy of the hybridized bonding plasmon mode.

26

TABLE OF CONTENTS

We demonstrate the direct detection of microRNA-210, a biomarker for hypoxia-related diseases, in cellular RNA extracts and cell media using discrete actuatable plasmonic nanoparticle dimers.

27